J Therm Anal Calorim (2009) 97:1015–1021
DOI 10.1007/s10973-009-0007-6

Phase diagram and electrical conductivity of the $CeBr_3$–CsBr binary system

Leszek Rycerz · Ewa Ingier-Stocka · Marcelle Gaune-Escard

Received: 7 May 2009 / Accepted: 7 May 2009 / Published online: 24 June 2009

Abstract Phase equilibrium in the $CeBr_3$–CsBr binary system was established from differential scanning calorimetry (DSC). This system includes three compounds, namely Cs_3CeBr_6, Cs_2CeBr_5 and $CsCe_2Br_7$; and three eutectics located at $CeBr_3$ molar fraction $x = 0.125$; 0.459 and 0.700, respectively. Cs_3CeBr_6 undergoes a solid–solid phase transition at 712 K and melts congruently at 1034 K. Cs_2CeBr_5 decomposes in the solid state into Cs_3CeBr_6 and $CsCe_2Br_7$ at 685 K. The third compound, $CsCe_2Br_7$, melts congruently at 877 K. The electrical conductivity of $CeBr_3$–CsBr liquid mixtures was measured down to temperatures below solidification over the whole composition range. Results obtained are discussed in term of possible complex formation.

Keywords Alkali halide · Compound · $CeBr_3$ · CsBr · Differential scanning calorimetry · Electrical conductivity · Lanthanide halide · Liquid complex · Melting · Phase diagram · Solid state transition

Electronic supplementary material The online version of this article (doi:10.1007/s10973-009-0007-6) contains supplementary material, which is available to authorized users.

L. Rycerz · E. Ingier-Stocka
Chemical Metallurgy Group, Faculty of Chemistry, Wroclaw University of Technology, Wybrzeze Wyspianskiego 27, 50-370 Wroclaw, Poland

M. Gaune-Escard (✉)
Ecole Polytechnique, Mecanique Energetique, Technopole de Chateau-Gombert, 5 rue Enrico Fermi, 13453 Marseille Cedex 13, France
e-mail: mge@polytech.univ-mrs.fr; Molten.Salts@polytech.univ-mrs.fr

Introduction

Phase equilibria in the LnX_3–MX lanthanide halide–alkali metal halide systems are generally complex and characterised by the existence of several stoichiometric compounds. While these systems have relatively simple phase diagrams for light alkali metal halides (LiX and NaX), those including KX, RbX and CsX exhibit several compounds of stoichiometry M_3LnX_6, M_2LnX_5 and MLn_2X_7. The stability of these compounds depends both on the nature of cations (lanthanide Ln, alkali metal M) and of the halide X [1–3]. As reported previously [3], a relation between the phase diagram topology and physicochemical properties of components was established. The so-called ionic potential, $IP = e_i/r_i$, where r_i = ionic radius, $e_i = Z_i\varepsilon$ (Z_i = valency, ε = elementary charge), was found to be an important parameter in this respect. The "ionic potential" is a measure of the electric field intensity at the cation surface, therefore accounting for interaction forces between cations with anions. The ionic potential ratio of the alkali metal cation and the lanthanide cation, IP_{M+}/IP_{Ln3+}, expresses a comparison of the interaction energies and influences the phase diagram topology of LnX_3–MX binary systems [3]. When $IP_{M+}/IP_{Ln3+} \leq 0.256$, both incongruently and congruently melting compounds are present in the systems.

This empirical classification was tested on earlier unknown $CeBr_3$–MBr binary systems (M = Li, Na, K, Rb). Indeed an excellent agreement was found since $CeBr_3$–LiBr and $CeBr_3$–NaBr are simple eutectic systems [4] ($IP_{M+}/IP_{Ce3+} = 0.465$ and 0.366, respectively), whereas in the system $CeBr_3$–KBr two congruently melting compounds [5], namely K_3CeBr_6 and K_2CeBr_5, exist ($IP_{K+}/IP_{Ce3+} = 0.249$). The $CeBr_3$–RbBr binary system ($IP_{Rb+}/IP_{Ce3+} = 0.231$) also follows the same rule: three

compounds [6] are formed; Rb_2CeBr_5 melts incongruently, while Rb_3CeBr_6 and $RbCe_2Br_7$ melt congruently.

This present work was devoted to the $CeBr_3$–CsBr binary system. A detailed DSC investigation highlighted the features of phase equilibrium. In addition electrical conductivity determination of liquid mixtures was conducted and is discussed in terms of possible complex formation.

Experimental

Sample preparation

Cerium(III) bromide was synthesised from the cerium(III) carbonate hydrate (Aldrich 99.9%). $Ce_2(CO_3)_3 \cdot xH_2O$ was dissolved in hot concentrated HBr acid. Solution was evaporated and $CeBr_3 \cdot xH_2O$ was crystallized. Ammonium bromide was then added and this wet mixture of hydrated $CeBr_3$ and NH_4Br was first slowly heated up to 450 and then up to 570 K to remove the water. Resulting mixture was subsequently heated to 650 K for sublimation of NH_4Br. Finally the salt was melted at 1100 K. Crude $CeBr_3$ was purified by distillation under reduced pressure ($\sim$0.1 Pa) in a quartz ampoule at 1150 K. $CeBr_3$ prepared in this way was of a high purity—min. 99.9%. Chemical analysis was performed by mercurimetric (bromine) and complexometric (cerium) methods. The results were as follows: Ce, 36.91 $\pm$ 0.03% (36.89% theoretical); Br, 63.09 $\pm$ 0.04% (63.11% theoretical).

Cesium bromide was Merck Suprapur reagent (min. 99.9%). Prior to use, it was progressively heated up to fusion under gaseous HBr atmosphere. HBr in excess was then removed from the melt by argon bubbling.

The mixtures of $CeBr_3$ and CsBr (in appropriate proportions) were melted in vacuum-sealed quartz ampoules in an electric furnace. Melts were homogenised by shaking and solidified. These samples were ground in an agate mortar in a glove box. Homogenous mixtures of different composition prepared along the same procedure were used both in phase diagram and electrical conductivity measurements.

All chemicals were handled in an argon glove box with a measured volume fraction of water of about 2×10^{-6} and continuous gas purification by forced recirculation through external molecular sieves.

Measurements

The temperatures and enthalpies of phase transitions of $CeBr_3$–CsBr binary mixtures were measured with a Setaram DSC 121 differential scanning calorimeter. The apparatus and the measurement procedure were described in details [2, 3]. Samples (300–500 mg) were contained in vacuum-sealed quartz ampoules (about 6 mm diameter, 15 mm length). Enthalpies of transition measurements were conducted at heating and cooling rates between 1 and 5 K min^{-1}. Some experiments were also performed at 0.1 K min^{-1} cooling rate.

Electrical conductivity measurements were carried out in capillary quartz cells with cylindrical platinum electrodes, described in details elsewhere [7]. These cells were calibrated at high temperature with pure molten NaCl [8]. The cell, filled with the substance under investigation, was placed into a furnace in a stainless steel block, used to achieve a uniform temperature. The conductivity of the melt was measured by platinum electrodes with the conductivity meter Tacussel CDM 230 during increasing and decreasing temperature runs. The mean values of these two runs were used in calculations. Experimental runs were performed at heating and cooling rates 1 K min^{-1}. The temperature was measured with a Pt/Pt–Rh(10) thermocouple with 1 K accuracy. Temperature and conductivity data acquisition was made with PC computer, interfaced to the conductivity meter. All measurements were carried out under static argon atmosphere. The accuracy of the measurements was about $\pm$2%.

Results and discussion

$CeBr_3$–CsBr phase diagram

The $CeBr_3$–CsBr phase diagram was established for the first time in the course of the present work. The DSC investigations were performed on samples with different compositions; the fusion temperature and enthalpy of the related mixtures were obtained from the corresponding curves. The enthalpies of thermal effects obtained from heating and cooling runs were almost the same (difference less than 2%). However, supercooling was observed on cooling curves and hence temperature and enthalpy data were obtained from heating curves only. All results are presented in Table 1.

In all DSC curves, the effect at highest temperature corresponds to liquidus. In the composition range $0 < x \leq 0.250$, where x is molar fraction of $CeBr_3$, two additional endothermic peaks were also present. The first one, at 842 K (mean value from measurements), is observable in all DSC curves up to $x < 0.250$ and can be undoubtedly ascribed to the CsBr–Cs_3CeBr_6 eutectic. Its disappearance from $x = 0.250$ suggests the existence of Cs_3CeBr_6 compound. The eutectic composition was determined accurately from the Tamman plot (Fig. 1a). The analysis of this experimental enthalpy vs. composition plot evidences that no solid solutions form in the system

Table 1 Results of the DSC experiments performed on the $CeBr_3$–CsBr binary system: T_1—Cs_3CeBr_6 transition, T_2—CsBr-Cs_3CeBr_6 eutectic, T_3—Cs_3CeBr_6–$CsCe_2Br_7$ eutectic, T_4—$CsCe_2Br_7$–$CeBr_3$ eutectic, T_5—Cs_2CeBr_5 decomposition, T_6—$CsCe_2Br_7$ transition, T_7—liquidus temperature

x, $CeBr_3$	T_1/K	T_2/K	T_3/K	T_4/K	T_5/K	T_6/K	T_7/K
0	–	–	–	–	–	–	909
0.025	698	837	–	–	–	–	905
0.050	700	842	–	–	–	–	891
0.075	708	843	–	–	–	–	879
0.093	708	843	–	–	–	–	855
0.121	712	844	–	–	–	–	852
0.149	715	843	–	–	–	–	927
0.171	716	842	–	–	–	–	961
0.199	717	840	–	–	–	–	998
0.222	719	839	–	–	–	–	1023
0.25	720	–	–	–	–	–	1034
0.266	717	–	740	–	688	–	1032
0.320	717	–	751	–	688	–	995
0.349	716	–	752	–	688	–	956
0.365	716	–	752	–	688	–	944
0.387	717	–	754	–	687	–	926
0.423	715	–	753	–	687	–	823
0.456	713	–	753	–	685	–	764
0.500	713	–	753	–	685	–	790
0.542	711	–	754	–	685	–	823
0.578	706	–	749	–	686	–	842
0.613	703	–	752	–	684	841	863
0.626	705	–	748	–	681	842	872
0.655	706	–	744	–	679	841	872
0.6589	707	–	743	–	679	841	874
0.666	–	–	–	–	–	841	877
0.670	–	–	–	–	–	841	875
0.680	–	–	–	857	–	841	871
0.696	–	–	–	859	–	841	859
0.706	–	–	–	856	–	840	856
0.715	–	–	–	856	–	840	871
0.722	–	–	–	858	–	840	883
0.757	–	–	–	857	–	841	904
0.786	–	–	–	857	–	842	924
0.860	–	–	–	855	–	839	970
0.908	–	–	–	857	–	840	985
0.975	–	–	–	848	–	841	1004
1	–	–	–	–	–	–	1006

rich in Cs_3CeBr_6. Thus the corresponding straight line intercepts the composition axis at $x = 0.250$; however, the formation of solid solutions cannot be excluded in the CsBr-rich side. Accordingly, the corresponding straight line was not forced to intercept the composition axis at $x = 0$. The eutectic composition ($x = 0.125$) was

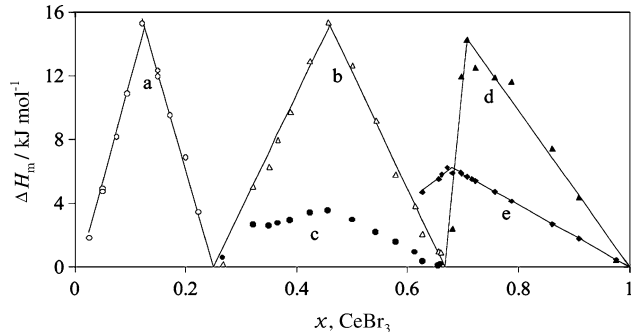

Fig. 1 Tamman construction for characteristic features determination in the CsBr–$CeBr_3$ system: (*a*) CsBr–Cs_3CeBr_6 eutectic; (*b*) Cs_3CeBr_6–$CsCe_2Br_7$ eutectic; (*c*) solid–solid transition in Cs_3CeBr_6; (*d*) $CsCe_2Br_7$–$CeBr_3$ eutectic; (*e*) solid–solid transition in $CsCe_2Br_7$; *symbols* experimental results, *solid lines* linear fitting of experimental results

determined from the intercept of the two linear parts in Fig. 1a, described by the equations:

$$\Delta_{fus}H_m = -1.071 + 128.323x$$

and $\Delta_{fus}H_m = 30.097 - 120.39x$ (in kJ mol^{-1}), x denotes molar fraction of $CeBr_3$).

The eutectic temperature determined from all appropriate DSC curves was found to be 842 K, whereas the enthalpy of fusion at the eutectic composition was equal to 15.0 kJ mol^{-1}. The molar fractions of CsBr at which solid solutions may exist at 668 K was found also from the Tamman diagram (Fig. 1a) as $x \leq 0.008$.

The second thermal effect observed at 712 K (mean value for all samples) in the composition range $0 < x \leq 0.250$ also occurs in all samples with $CeBr_3$ molar fractions up to $x < 0.666$, composition at which it disappears. This corresponds to the solid–solid transition in Cs_3CeBr_6 compound. The molar enthalpy related to this effect (calculated for the Cs_3CeBr_6 compound) 8.0 kJ ml^{-1} is in excellent agreement with the enthalpy observed for solid–solid phase transition in many M_3LnX_6 compounds (M = Rb, Cs; Ln = lanthanide) [2, 3]. The two thermal events observed in the mixture of composition $x = 0.250$ are related to a solid–solid transition and congruent melting of Cs_3CeBr_6.

No effect could be observed at 712 K for the sample with $x = 0.666$, thus suggesting the existence of another compound, namely $CsCe_2Br_7$. Indeed, the thermal effects observed in the composition range $0.250 < x < 0.666$ differ significantly from those corresponding to the $0.666 < x < 1$ composition range. In addition at the composition $x = 0.666$ only one endothermic peak, characteristic of congruent melting, was observed. This confirms the existence of the congruently melting $CsCe_2Br_7$ compound in the $CeBr_3$–CsBr binary system.

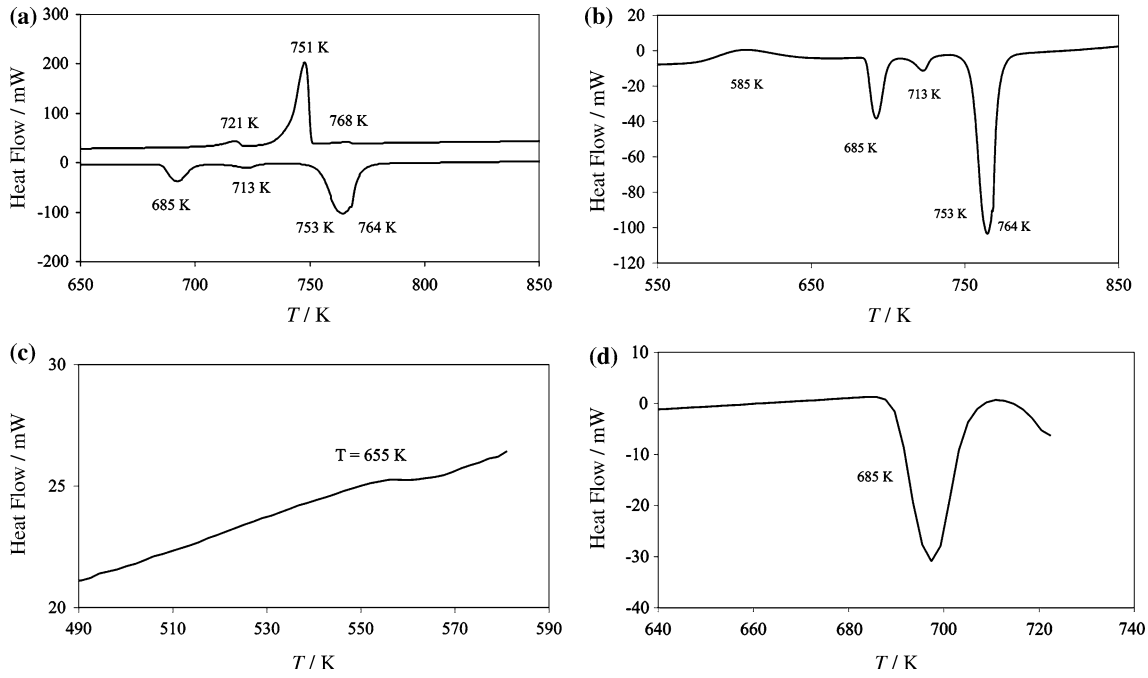

Fig. 2 Experimental thermograms: **a** primary heating/cooling (5 K min^{-1}); **b** secondary heating (5 K min^{-1}); **c** Cs_3CeBr_5 formation on slow cooling (0.1 K min^{-1}); **d** subsequent heating

On heating curves of samples in the range $0.250 < x < 0.613$, three endothermic peaks were observed in addition to liquidus. At $CeBr_3$-richer compositions, an additional endothermic effect is visible at 841 K at all compositions $0.613 < x < 1$. The first effect at 750 K (mean value) corresponds to the Cs_3CeBr_6–$CsCe_2Br_7$ eutectic. The enthalpy related to this effect was plotted against composition in Fig. 1b. The eutectic composition was determined from the intercept of the two linear parts as $x = 0.459$. The melting enthalpy, $\Delta_{fus}H_m$, 15.1 kJ mol^{-1}, is related to this eutectic mixture. In this Tamman construction it was assumed that there was no solubility in the solid state. Thus the straight lines intercept the composition axis at $x = 0.250$ and 0.666.

The second thermal effect at 712 K that appears in the composition range $0.250 < x < 0.666$, corresponds to the solid–solid transition in Cs_3CeBr_6, as discussed above. The third one, at 685 K corresponds to the decomposition in the solid state of another compound. The corresponding Tamman diagram (enthalpy *vs*. composition) does not give any clear information about the composition of this compound (Fig. 1c). One can anticipate that it may be Cs_2CeBr_5 [1–3], by comparison with several LnX_3–CsX systems.

In addition very interesting phenomena were observed on DSC curves for samples with composition $0.250 < x < 0.666$ (Fig. 2). On primary heating curves (heating rate 5 K min^{-1}), an endothermic effect was visible at 685 K at all compositions, which was assessed to possible decomposition of $CsCeBr_5$ into the adjacent Cs_3CeBr_6 and $CsCe_2Br_7$ compounds. However, on subsequent cooling, the formation of Cs_3CeBr_5 was not observed (Fig. 2a) and it is likely that a metastable mixture of Cs_3CeBr_6 and $CsCe_2Br_7$ exists down to room temperature instead. Reconstructive phase transitions are special kinds of solid–state reactions in which the arrangements of the ions are drastically changed. Ions have to move from one site to another passing strong potential walls of other ions. The resulting "kinetic hindrance" can cause a great difference between reaction temperatures, measured in DSC heating and cooling runs (thermal hysteresis) [9]. In extreme cases during cooling experiments the "undercooling" can become so strong that the reaction does not occur in the DSC time-scale. Due to kinetic reasons, the compound formation during cooling does not take place and a metastable mixture of other compounds exists instead. Thus secondary heating runs were performed at heating rate 5 K min^{-1} and this time an exothermic effect was observed first at about 585 K which was followed by an endothermic effect (Fig. 2b) occurring at a temperature identical to that of decomposition previously observed (685 K). But on this secondary cooling curve, the effect at 685 K (compound formation) was once again not visible. So, we decided to heat once again one sample up to melting and to cool it down to room temperature, but at a very low cooling rate (0.1 K min^{-1}). This time the effect corresponding to the compound formation was observed at about 655 K (Fig. 2c). As the compound was formed during cooling, no exothermic effect was

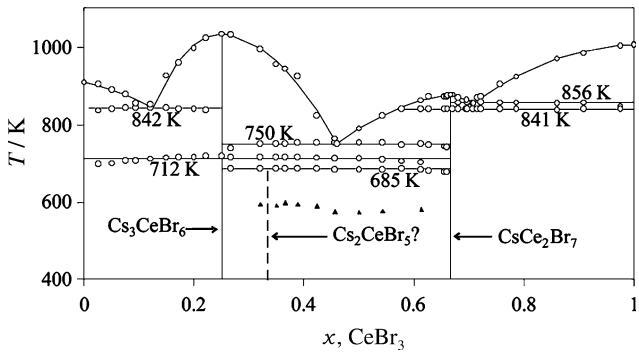

Fig. 3 Phase diagram of the CsBr–$CeBr_3$ system

present in subsequent heating DSC curve (Fig. 2d). As mentioned above, the compound composition could not be determined precisely from Tamman diagram. The reason of this unusual situation can be related to the existence of metastable phases, the enthalpy of which could not be measured accurately. X-ray structural measurements which are planned in the near future, would confirm or exclude the existence of this postulated Cs_2CeBr_5 compound.

The fourth thermal endothermic effect, at 841 K, which appears for $x \geq 0.613$ is related to a solid–solid transition in the $CsCe_2Br_7$ compound.

Two effects in addition to liquidus are observed in the composition range $0.666 < x < 1$. The first one at 841 K corresponds, as stated above, to the solid–solid transition in $CsCe_2Br_7$ compound. The molar enthalpy related to this effect was plotted against composition in Fig. 1e. The compound composition, $x = 0.679$, determined from intercept of the two straight lines in this figure is in good agreement with the theoretical value $x = 0.666$ for $CsCe_2Br_7$. The second effect at about 856 K corresponds to the $CsCe_2Br_7$–$CeBr_3$ eutectic. The enthalpy related to this effect was plotted against composition in Fig. 1d. The eutectic composition, $x = 0.708$, was found from the diagram in Fig. 1c. The melting enthalpy at 856 K, $\Delta_{fus}H_m$, 14.3 kJ mol^{-1} was related to the eutectic mixture. In the Tamman construction it was assumed that there was no solubility in the solid state. Thus the straight lines intercept the composition axis at $x = 0.666$ and $x = 1$. It is very likely that the exothermic effect corresponds to the hindered formation of the Cs_2CeBr_5 compound.

The phase diagram constructed from this whole experimental information is displayed in Fig. 3.

Electrical conductivity

The electrical conductivity, κ, of $CeBr_3$–CsBr liquid mixtures was measured for the first time. Experimental determinations were conducted over the entire composition range in steps of about 10 mol%. The specific conductivity, κ, of each mixture showed deviation from linearity when plotted against temperature as $\ln(\kappa) = f(1/T)$. Such a deviation from the classical Arrhenius equation was already mentioned in literature [10]. Thus the following Eq. (1) was used to fit experimental conductivity data:

$$\ln(\kappa) = A_0 + A_1 \cdot 10^3 \cdot \left(\frac{1}{T}\right) + A_2 \cdot 10^6 \cdot \left(\frac{1}{T}\right)^2 \quad (1)$$

where A_0, A_1, and A_2 are coefficients determined by the least-squares method.

The E_A activation energy, evaluated by analogy to the Arrhenius equation as

$$E_A(T) = -R\frac{d\ln(\kappa)}{d\left(\frac{1}{T}\right)} \quad (2)$$

where R is the gas constant, becomes:

$$E_A = -R\left[A_1 + 2A_2\left(\frac{1}{T}\right)\right] \quad (3)$$

All A_i coefficients are listed in Table 2, together with the E_A values determined at 1050 K for all the $CeBr_3$–CsBr mixtures.

The experimental conductivity isotherm at 1050 K was plotted against the mole fraction of $CeBr_3$ in Fig. 4. For comparison, the isotherms (at the same temperature), relative to other $CeBr_3$–MBr (M = Li, Na, K, Rb) systems [4–6], are also presented. Electrical conductivity decreases with increasing radius of the alkali metal cation i.e. from lithium to cesium. In all systems the specific conductance decreases with increasing $CeBr_3$ concentration, with significantly larger conductivity changes in the alkali bromide-rich region. We had observed a similar behaviour in many other lanthanide halide–alkali metal halide binary systems [4–6, 9, 10].

As indicated above, the activation energy for conductivity changes with temperature in every individual mixture, validating the early statement made by Yaffe and van Artsdalen [11, 12] of a correlation with structural changes in melts.

Raman spectroscopic investigations [13] showed that octahedral $LnBr_6^{3-}$ ions are formed in the $LnBr_3$–MBr liquid mixtures. These ions constitute the predominant species in the MBr-rich liquid mixtures. As the $LnBr_3$ concentration increases distorted octahedral species occurs, which are bridged by bromide anions. The formation of these $CeBr_6^{3-}$ complexes influences the electrical conductivity vs. composition plot (Fig. 4). Complex formation in the melt also influences the activation energy for electrical conductivity, which should increase with increasing amount of complex formed. This was observed indeed in the system under discussion as in the other $CeBr_3$–MBr mixtures. However, some differences were found between $CeBr_3$–LiBr and $CeBr_3$–NaBr on the one hand, and the other $CeBr_3$–MBr systems, on the other. Figure 5 shows the activation energy

Table 2 Coefficients in equation: $\ln \kappa = A_0 + A_1\ (1{,}000/T) + A_2(1{,}000/T)^2$ and activation energy of the electrical conductivity (E_A) of liquid $CeBr_3$–CsBr binary mixtures at 1,050 K: κ in S m^{-1}, ln(*s*)—standard deviation of ln κ, *n* = number of experimental data points

x, $CeBr_3$	Temperature range (K)	A_0 (S m^{-1})	A_1 (S m^{-1} K)	A_2 (S m^{-1} K^2)	ln(*s*)	*n*	E_A at 1,050 K (kJ/mol)
0.065	897–1160	5.0542	0.6130	−1.1844	0.0021	580	13.71
0.126	896–1160	5.1202	0.3954	−1.1894	0.0021	548	15.76
0.204	1029–1160	4.7235	1.1573	−1.7661	0.0011	326	18.41
0.300	1036–1120	4.6174	1.1295	−1.8188	0.0017	341	19.48
0.399	921–1120	4.5249	0.9836	−1.6735	0.0012	921	18.39
0.497	813–1120	3.7261	2.6998	−2.5890	0.0042	1134	18.62
0.649	884–1120	3.1996	4.7048	−4.0073	0.0022	603	24.43
0.749	903–1120	3.8179	3.7582	−3.5862	0.0069	441	25.64
0.802	978–1160	4.2558	3.1450	−3.4169	0.0010	813	28.06
0.849	960–1120	4.1603	3.3048	−3.4489	0.0030	423	27.24
0.893	980–1120	5.1253	1.3478	−2.4402	0.0032	307	27.53
0.908	996–1160	4.9484	1.6673	−2.5993	0.0016	714	27.39
0.952	998–1120	5.2123	1.2256	−2.3754	0.0034	312	27.52
1.000	988–1123	0.0014	12.2264	−8.1698	0.0095	1345	27.73

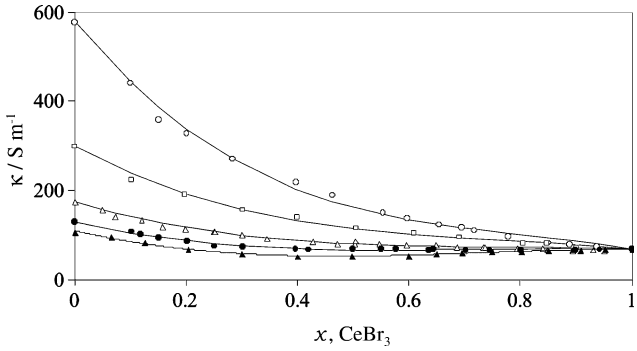

Fig. 4 Experimental conductivity isotherm at 1,050 K: *open circles* LiCl–$CsBr_3$; *open squares* NaCl–$CsBr_3$; *open triangles* KBr–$CsBr_3$; *black circles* RbCl–$CsBr_3$; *black triangles* CsBr–$CsBr_3$

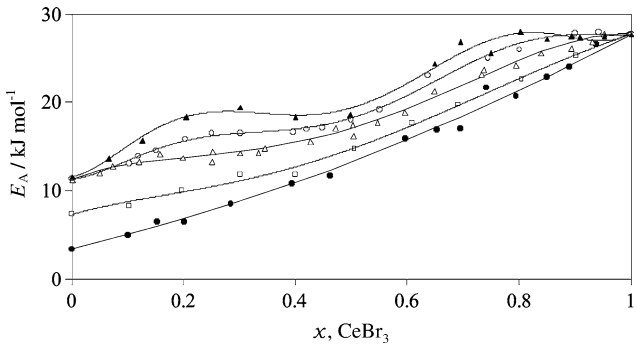

Fig. 5 Activation energy at 1,050 K as a function of composition for the $CeBr_3$–MBr systems (M = Li, Na, K, Rb, Cs): *black circles* LiCl–$CsBr_3$; *open squares* NaCl–$CsBr_3$; *open triangles* KBr–$CsBr_3$; *white circles* RbCl–$CsBr_3$; *black triangles* CsBr–$CsBr_3$

at 1050 K as a function of composition for the $CeBr_3$–MBr systems (M = Li, Na, K, Rb, Cs). Whereas in the systems with LiBr and NaBr the activation energy increases smoothly with $CeBr_3$ concentration, in the systems with KBr, RbBr and especially with CsBr it increases up to about 20 mol% of $CeBr_3$ and become almost stable up to 50 mol% of $CeBr_3$. This plateau can be explained in terms of different forms of complexes which co-exist as evidenced by Raman spectroscopy [13].

The activation energy for electrical conductivity increases with alkali metal cationic radius (from lithium to cesium). It is likely that this is due to complex concentration increase in the melt. This observation is in agreement with mixing enthalpy measurements performed on $CeBr_3$–MBr systems [14–16], that also showed that formation enthalpy, attributed to the $CeBr_6^{3-}$ complex ions formation, increases with ionic radius of alkali metal cation. The role of alkali bromides is to provide additional bromide ions to enable Ce^{3+} to expand its coordination shell. But there is competition between M^+ and Ce^{3+} for Br^- in the ionic environment. The result of this competition depends on the relative attracting power of the alkali ion. Li^+ is the most halide attracting and Cs^+ the least. The radius of the alkali metal will therefore govern the complex ion formation in $CeBr_3$–MBr binary systems. Thus the presence of CsBr in mixtures with $CeBr_3$ favours complex ion formation more than addition of RbBr (KBr, NaBr, LiBr) and results in a larger enthalpy of formation, larger activation energy for conductivity, etc.

Conclusion

The $CeBr_3$–CsBr binary system is characterized by three eutectics, the composition and melting temperature of which

were determined accurately, and three stoichiometric compounds, namely Cs_3CeBr_6, Cs_2CeBr_5 and $CsCe_2Br_7$. Cs_3CeBr_6 undergoes a solid–solid phase transition at 712 K and melts congruently at 1034 K. Cs_2CeBr_5 decomposes in the solid state into Cs_3CeBr_6 and $CsCe_2Br_7$ at 685 K. The third compound, $CsCe_2Br_7$, melts congruently at 877 K. The electrical conductivity of $CeBr_3$–CsBr liquid mixtures was measured below the solidification temperature over the whole composition range. Results obtained are discussed in term of possible complex formation.

Acknowledgements Financial support by the Polish Ministry of Science and Higher Education from budget on science in 2007–2010 under the grant N_N204 4098 33 is gratefully acknowledged. L.R. and E.I.-S. wish to thank the Ecole Polytechnique de Marseille for hospitality and support during this work.

References

1. Seifert HJ. Ternary chlorides of the trivalent early lanthanides. Phase diagrams, crystal structures and thermodynamic properties. J Therm Anal Cal 2002;67:789–826.
2. Rycerz L. High temperature characterization of LnX_3 and LnX_3-AX solid and liquid systems (Ln = Lanthanide, A = Alkali, X = Halide): thermodynamics and electrical conductivity. Ph. D. Thesis, Marseille; 2003.
3. Rycerz L. Thermochemistry of lanthanide halides and compounds formed in lanthanide halide-alkali metal halide systems (in Polish). Scientific Papers of Institute of Inorganic Chemistry and Metallurgy of Rare Elements, Wroclaw University of Technology, Series Monographs 35, Wroclaw; 2004.
4. Ingier-Stocka E, Rycerz L, Gadzuric S, Gaune-Escard M. Thermal and conductometric studies of the $CeBr_3$-MBr binary systems (M = Li, Na). J Alloys Comp 2008;450:162–6.
5. Rycerz L, Ingier-Stocka E, Gadzuric S, Gaune-Escard M. Phase diagram and electrical conductivity of $CeBr_3$-KBr. Z Naturforsch 2007;62a:197–204.
6. Rycerz L, Ingier-Stocka E, Gadzuric S, Gaune-Escard M. Phase diagram and electrical conductivity of the $CeBr_3$-RbBr binary system. J Alloys Comp 2008;450:175–180.
7. Fouque Y, Gaune-Escard M, Szczepaniak W, Bogacz A. Syntheses, measures des conductibilites electriques et des entropies de changements d'etat pour le compose Na_2UBr_6. J Chim Phys 1978;75:361–6.
8. Janz GI. Thermodynamic and transport properties for molten salts; correlation equations for critically evaluated density, surface tension, electrical conductance, and viscosity data. J Phys Chem Ref Data. 1988;17 Suppl 2:232
9. Seifert HJ. Ternary chlorides of the trivalent late lanthanides. J Therm Anal Cal 2006;83:479–505.
10. Potapov A, Gaune-Escard M. Deviations from the Arrhenius equation of electrical conductivity polytherms. In: Øye HA, Jagtøyen A, editors. Proccedings of the International Symposium on ionic liquids in honour of Professor Marcelle Gaune-Escard. Carry le Rouet, France; 2003, June 26–28. pp. 477–81.
11. Gadzuric S, Ingier-Stocka E, Rycerz L, Gaune-Escard M. Electrical conductivity of molten binary $NdBr_3$-alkali bromide mixtures. Z Naturforsch 2004;59a:77–83.
12. Ziolek B, Rycerz L, Gadzuric S, Ingier-Stocka E, Gaune-Escard M. Electrical conductivity of molten $LaBr_3$–MBr binary mixtures. Z Naturforsch 2005;60:75–80.
13. Van Artsdalen ER, Yaffe JS. Electrical conductance and density of molten salt systems: KCl-LiCl, KCl-NaCl and KCl-KI. J Phys Chem 1955;59:118–27.
14. Yaffe JS, van Artsdalen ER. Electrical conductance and density of pure molten alkali halides. J Phys Chem 1956;60:1125–31.
15. Photiadis GM, Borresen B, Papatheodorou GN. Vibrational modes and structures of lanthanide halide–alkali halide binary melts; $LnBr_3$-KBr (Ln = La, Nd, Gd) and $NdCl_3$-ACl (A = Li, Na, K, Cs). J Chem Soc Faraday Trans 1998;17:2605–13.
16. Rycerz L, Gaune-Escard M. Unpublished results.